Inorganic Chemistry Frontiers 5.1 (2018): 73-83

DOI: http://doi.org/10.1039/C7QI00446J

View Article Online
DOI: 10.1039/C7QI00446J

Journal Name

ARTICLE

Mononuclear Pd(II) and Pt(II) complexes with an α-N-heterocyclic thiosemicarbazone: cytotoxicity, solution behaviour and interaction versus proven models from the biological media

Received 00th January 20xx,
Accepted 00th January 20xx

DOI: 10.1039/x0xx00000x

www.rsc.org/

Ana I. Matesanz[a]; Eva Jimenez-Faraco[a]; María C. Ruiz[b]; Lucia M. Balsa[b] ; Carmen Navarro-Ranninger[a]; Ignacio E. León[b]*; A.G. Quiroga[a]*

Two Pd(II) and Pt(II) complexes with two pyrrol-2-carbaldehyde N-p-chlorophenylthiosemicarbazone ligands are designed and characterized showing mononuclear structures. An important pharmacological property for both compounds is the high selectivity for tumor cells and a lack of activity in healthy cells. The Pd(II) compound shows higher antitumor activity and selectivity than the Pt(II) compound. Both complexes present a variety of biological interactions: with DNA models (pBR322 and CT DNA), proteins (lysozyme and RNase) and other biological targets like proteosome. Our results show that the Pd(II) complex is a more interesting candidate for potential anticancer therapies than the Pt(II) complex, and we provide new insight into the design and synthesis of palladium compounds as potential antitumor agents.

Introduction

Thiosemicarbazone ligands (TSCN) are molecules with an established history as pharmacological agents, not only for their biological properties but also because of their great capacity for binding with metals. Triapine® is a thiosemicarbazone containing an N-heterocyclic ring and is of special interest because of its multiple clinical trial studies[1, 2]. Triapine® is currently included in a Phase 2 of an ongoing clinical trial for the treatment of non-localized cervical cancer at the National Cancer Institute.[3] The most accepted hypothesis regarding TSCN antitumoral action is based in their chelating properties, which indirectly lead to study ribonucleotide reductase (RR) as the mechanism through which these molecules work.[4] RR is an iron-dependent enzyme that promotes the reduction of ribose to deoxyribose. Some TSCNs' affect RR inhibition and lead to the blockage of the synthesis phase of the cell cycle and eventually to cell death by apoptosis.[5]

α-N-heterocyclic thiosemicarbazones turned out to be the most potent inhibitors of RR so far,[6] and the identification of its metal coordination was reported to afford more active species than free ligands.[7] Recent studies have shown that the methylation of Triapine®results in a change of the mode of action, which might be associated with its possible interaction with copper caused by the balance of the intracellular copper concentration. However, these effects do not seem to be responsible for the increased cytotoxic activity of some derivatives into the nanomolar range.[8]

Para-substituted phenyl thiosemicarbazones are another example of strong antitumor compounds and their metallation using palladium and platinum are reported to afford complexes that highly enhance the antitumor action of the ligands. The data from these complexes showed a good correlation of their cytotoxic activity with their structures and mode of action.[9] By changing the structure of the complex, their interaction with DNA varies from cisplatin type of interaction to interstrand crosslinking.[10, 11] Heterocyclic TSCN are good candidates not only to afford platinum and palladium complexes,[12] but also complexes with some other metals such as copper[13, 14] and ruthenium.[15] The most remarkable results have been achieved so far with copper,[16, 17] iron and gallium[1] bound to Triapine®.

Following these results and trying to elucidate, if metal complexes from α-N-heterocyclic thiosemicarbazones can achieved more selectivity versus special tumor lines, we have developed a new series of metal complexes with pyrrol-2-carbaldehyde ^{4}N-*p*-chlorophenylthiosemicarbazone (LH_2) where the metal can be Pd(II) and Pt(II).

We seek not only selective and active compounds versus specific cancer cell lines such the human osteosarcoma MG-63 cell line.[18] We also search for compounds that might allow normal cell viability of non-tumoral cell lines "in vitro" (for example L929 fibroblast). In this work, we present new compounds and the studies of their cytotoxicity, structure and stability in solution, demonstrating their potential as antitumor drugs. The binding and/or affinity to biological models such two model proteins (lysozyme and RNase), proteasome and

[a] Dept. Química Inorgánica and IAdChem (Institute for Advanced Research in Chemical Science) Universidad Autónoma de Madrid. 28045 Madrid. Spain.
[b] Centro de Química Inorgánica (CEQUINOR, CONICET), Facultad de Ciencias Exactas, Universidad Nacional de La Plata, 47 y 115, 1900 La Plata, Argentina

† Electronic Supplementary Information (ESI) available: [NMR and UV spectra, images of genotoxicity effect, ROS production values in Jurkat cells]. See DOI: 10.1039/x0xx00000x

View Article Online
DOI: 10.1039/C7QI00446J

DNA, indicates a different mode of action to the classical metallodrugs, such as cisplatin.

Results and discussion

Chemistry

Scheme 1 shows the synthesis of the thiosemicarbazone, pyrrol-2-carbaldehyde ^{4}N-*p*-chlorophenylthiosemicarbazone (LH_2). The synthesis began with ^{4}N-*p*-chlorophenyl thiosemicarbazide preparation, using stoichiometric amounts of *p*-chlorophenyl isothiocyanate and hydrazine monohydrate. The procedure to synthesize thiosemicarbazones was reported in the fifties and proceeds by the condensation of the aldehyde and the corresponding thiosemicarbazide.[19] This procedure has been used for obtaining a broad number of thiosemicarbazones derivatives[12]. The experimental section includes the detailed procedure used for the synthesis of LH_2. The Pd(II) complex **1**, was synthesized using Li_2PdCl_4, prepared in situ from palladium(II) chloride and lithium chloride (1:2) in MeOH,[20] then reacted with the stoichiometric amount of LH_2 at room temperature to afford complex **1**.

The low solubility of complex **1** allowed to obtain low concentrated DMSO solutions that easily led to single crystals suitable for X-ray diffraction structure resolution. We used crushed and vacuum dried single crystals samples for full characterization and biological assays. IR, NMR and analysis data are in agreement with the structure of the complex finally solved by X-Ray diffraction (Figure 1).

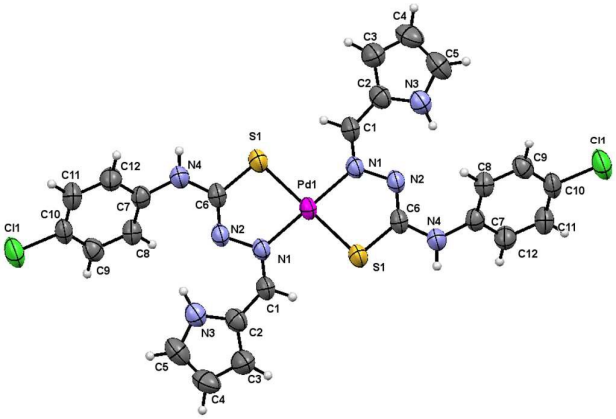

Figure 1. X-Ray structure of complex **1**

The structure of complex **1** consists of discrete molecules that correspond to $[Pd(LH)_2]\cdot 2DMSO$ unit. The geometry around the metal ion is square planar being the palladium atom bound to the sulfur and azomethine nitrogen atoms of the two mutually *trans,* deprotonated thiosemicarbazone ligands. The asymmetric unit only contains one-half of the complex **1** molecule, with the palladium atom located on a crystallographic inversion centre, together with one DMSO molecule. The distances and angles around the Pd atom are within the range expected for these kind of mononuclear[21] and other polynuclear complexes published previously by our group of research[10](Table 1).

Table 1. Selected bond distances and angles for $[Pd(LH)_2]\cdot 2DMSO$

Bond distances (Å)		Bond distances (Å)		Bond angles (º)	
Pd1-N1	2.023(3)	C6-N2	1.296(5)	N1-Pd1-N1	180.0
Pd1-S1	2.2731(12)	C6-N4	1.357(5)	N1-Pd1-S1	83.33(8)
C1-N1	1.288(5)	C6-S1	1.736(4)	S1-Pd1-S1	180.0
C2-N3	1.364(5)	C7-N4	1.410(5)		
C5-N3	1.340(5)	N1-N2	1.415(4)		

The synthesis of the platinum complex, **2** was similar to the one used for complex **1**, as shown in Scheme 1, but required the use of water to dissolve the starting material K_2PtCl_4. The characterization of complex **2** by the usual techniques indicated a general formula: $[Pt(LH)_2]$, similar to complex **1**. Unfortunately, none of single crystals achieved were adequate for X-ray characterization.

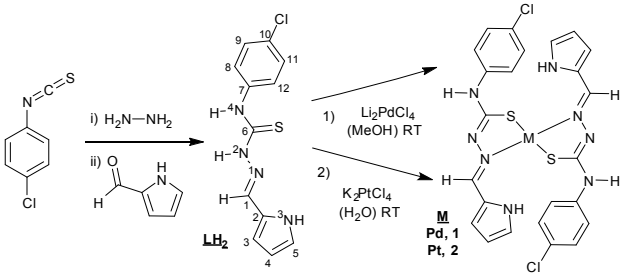

Scheme 1

The stability of both complexes was studied by ^{1}H NMR (fresh sample and 24h) in DMSO-d^6 (Figure SM1) and by UV in Trisbuffer:DMSO (95:5) (Figure SM2 and SM3). Complexes **1** and **2** behaviour in solution is very similar. The UV spectra showed no significant changes (no shifts of the λmax and no new peaks) other than a small decrease in absorbance values after 24h. Both complexes' (**1** and **2**) solutions are stable enough to be studied as potential metallodrugs within pH range = 6-8. Both complexes' (**1** and **2**) solutions are stable enough to be studied as potential metallodrugs within pH range = 6-8.

Cytotoxicity

Following our expectations to achieve a novel drug with specific activity versus cancer cell lines, both compounds **1** and **2** showed an antiproliferative activity values within 25-100 µM (table 2A) and 15-50 µM (Table 2B) for the following cell lines: Jurkat (human leukemia), MG-63 (human osteosarcoma) and A549 (human lung adenocarcinoma), remarkably none of the complexes showed such effect in normal mice fibroblast L929. Cisplatin showed a much higher cytotoxicity in this normal cell line phenotype (L929) compared with the new complexes cytotoxicity, and this particular effect enhances the potential value of complexes **1** and **2** as new metallodrugs in anticancer therapy.

View Article Online
DOI: 10.1039/C7QI00446J

The best candidate is the palladium derivative, complex **1**, which showed a lower IC_{50} in leukemic and osteosarcoma cell lines than the platinum derivative, complex **2**. The IC_{50} value of complex **1** in the lung cancer cell line A549 (see Table 2A, 60 μM) is a more remarkable data than the platinum complex value (100 μM) and is similar to cisplatin (62μM). Moreover, after 72 h of incubation, the IC_{50} value of complex **1** in A549 cells is 36 μM whilst for the platinum complex is 79 μM (see Table 2B).

Table 2A. IC_{50} values of complex **1** and **2** in several cell lines after 48h.

	L929(μM)	Jurkat(μM)	A549(μM)	MG-63(μM)
1, $Pd(LH)_2$	>100	47 ± 3	60 ± 3	34 ± 2
2, $Pt(LH)_2$	>100	63 ± 2	>100	56 ± 5
cisplatin	43 ± 4	8 ± 1	62 ± 5	33 ± 3

Table 2B. IC_{50} values of complex **1** and **2** in several cell lines after 72 h.

	L929(μM)	Jurkat(μM)	A549(μM)	MG-63(μM)
1, $Pd(LH)_2$	86 ± 4	17 ± 5	36 ± 3	20 ± 4
2, $Pt(LH)_2$	81 ± 3	33 ± 4	79 ± 4	32 ± 3
cisplatin	26 ± 3	4 ± 1	29 ± 5	17 ± 3

Table 2C shows the higher selectivity of compound **1** for A549 and MG-63 cells in comparison with compound **2** and cisplatin. The SI values are 2.46, 1.02, 0.90 (A549 cells) and 4.3, 2.3 and 1.5 (MG-63 cells) for compound **1**, **2** and cisplatin, respectively. Nevertheless, cisplatin showed a better correlation of SI on Jurkat cells than compound **1** and **2**.

Table 2C. SI (Selectivity Index) values of complexes **1**, **2** and cisplatin in several cell lines after 72h

	Jurkat	A549	MG-63
1, $Pd(LH)_2$	5	2.46	4.3
2, $Pt(LH)_2$	2. 4	1.02	2.5
cisplatin	6.5	0.90	1.5

SI (Selectivity index) is a comparison of the amount of a therapeutic agent that causes the therapeutic effect (on tumor cells) and amount that causes toxicity (using normal cells)

To our knowledge, there are very few examples in the references where the palladium thiosemicarbazone derivative showed better cytotoxicity than the platinum analogue.[22-24] In fact, this kind of response should not be that unusual in chelate complexes, based in the higher kinetic lability of the Pd(II) complexes[25], which should endow the complex with a better interaction potential with DNA or other biological molecules usually overexpressed in the cancer cells.

Reactivity versus biological molecules

Affinity of the complexes for the model CT DNA

Covalent binding with DNA is the reported mode of action of cisplatin like metallodrugs, via aquation of the leaving groups.[26] However, there are other antitumor active metal complexes keeping their ligands and their structure integrity in physiological solution, and those can interact with DNA by many different mechanism.[27, 28] Examples of such mechanism are: cleavage of the DNA-helix, non-covalent interaction, the intercalation by stacking in between the DNA-bases, electrostatic, hydrophobic or hydrogen bonding from different groups and substituents with the DNA and even van der Waals forces.[12, 29, 30]

The affinity of both complexes for CT DNA was evaluated using UV spectroscopy titrations, as a preliminary step to determine information concerning their possible targets and provide information about the mechanism. The typical β-form of DNA exhibit a characteristic π-π* band at 260nm, which is sensitive to structural changes in the macromolecule and can become hyperchromic (increase in absorption of the DNA band at 260 nm) by perturbation resulting from non-covalent external interaction.[31]

First, the UV spectra of a CT DNA solution (3.2×10^{-5} M) were monitored using increasing concentration of the complexes **1-2** (following different r values in table 3 and figure SM4)), allowing the sample to react for 10 minutes. The binding to CT DNA showed an increasing effect in the 260nm band; typically described for a hyperchromic effect (Table 3 collects the values). All of these data might indicate interaction of the complexes with CT-DNA that could be interpreted as an external non-covalent interaction, and no bathochromic effect is detected.[31]

Table 3. UV/Vis absorption data of complex **1** and **2** with CT DNA and their DNA-binding constants (Kb).

	Band (nm); A[a]	Hyperchromism %[b]	Kb (M^{-1})
CT-DNA	260 ; 021	-	-
Complex **1**	265; 0.44	37	$2.55 \cdot 10^5$
Complex **2**	266; 0.32	34	$3.99 \cdot 10^5$

[a] r=1,25=[complex]/[DNA]; [b] (%) = $100(A_{DNAbound}-A_{DNA\ free})/A_{DNA\ free}$

Secondly, the UV spectra of increasing concentration of CT DNA solution (3.2×10^{-5} M) were monitored using a fixed concentration of the complexes **1-2** (2.5×10^{-6}M, see figure SM5), allowing the sample to react for 10 minutes. The DNA-binding constants (Kb) of complexes **1** and **2** (Table 2) were determined by the plots [DNA]/(εa-εf) versus [DNA] (Fig. SM5) using the Wolfe-Shimer equation [32]. In brief, the Kb constants of the complexes **1** and **2** are comparable with those observed for classical groove binders (Table 3), such a as Hoechst 32258 with a $4.6 \bullet 10^5$ M^{-1} with A3T3 duplex [33].

These values, recorded in the first 10 minutes of reaction, seemed to indicate that the reactivity of these compounds could be interpreted as having a good affinity for CT DNA base pairs in a non-covalent binding mode of action. The reactivity observed is quite different to cisplatin, which is as a covalent binder reported to produce two effects: hyperchromic and bathochromic after 7h or reaction.[31]

Interaction of the complexes with the plasmid DNA supercoiled pBR322

Based in the best cytotoxicity values, we selected complex **1** to evaluate its interaction with a more specific model of DNA. We performed a study of its interaction with a supercoiled DNA pBR322 (containing two isoforms) used as a model of the

View Article Online
DOI: 10.1039/C7QI00446J

secondary structure of DNA. Cisplatin binds covalently to DNA and also to pBR322 producing a delay in its closed circular form (cc) and slowing down the open circular form (oc) because of its unwinding. [26, 34]

Complex **1** was assayed at different r_i concentrations after 24h.The electrophoresis results showed that complex **1** did not seem to alter the electrophoretic mobility of the plasmid, but we could barely detect a blur band in between the oc and ccc forms (data not shown). Several repetitions did not improve the visibility of such band that is why we allowed a longer time of reaction. After 48h (Figure 2), we could clearly detect a new band in lines 3 to 6 possibly caused by a nicked in one of the pBR322 form (marker and pBR322 control are in lines 1 and 2 respectively for better comparison). This assay manifests that complex **1** is able to produce a new band corresponding possibly to a new fragment. Complex **1** interaction with pBR322 showed a different mode of action compared to cisplatin.

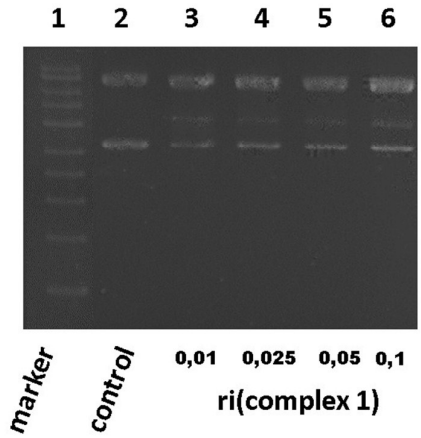

Figure 2. Electrophoresis in agarose gel of pBR322 plasmid treated with complex **1.** ri: metal complex:DNA base pairs. Line1: marker (DNA 1kb ladder) Line 2: C: control of incubated DNA plasmid pBR322, line 3 to 6: complex **1**: Plasmid DNA incubated at ri = 0.01 to 0.1.

Genotoxicity study

The genotoxic effects of complexes **1** and **2** were investigated through the induction of DNA damage. The single cell gel electrophoresis (SCGE) or comet assay is an important test used for the investigation of genotoxicity. It detects single and double strand DNA breaks. Sites where excision and repairs have occurred are detected under alkaline conditions.[35] For both complexes, we evaluated the tail moment parameter, which is defined as the tail length × DNA amount in the tail. The distance of DNA migration is used to measure the extent of DNA damage. However, if DNA damage is relatively high, the tail increases in fluorescent staining intensity but not in length.[36] Thus, for these reasons it is useful to use the tail moment as a genotoxic endpoint. As it is shown in Fig. 3A, complex **1** produced a significant genotoxic effect in Jurkat cells from 2.5 to 5 μM with a dose-response effects ($p < 0.001$). From 10 μM the genotoxic effect is less pronounced. The decrease in DNA damage as the complex concentration increases may be due to overt cytotoxicity exerted on this cell line. Moreover, the genotoxic effects of complex **1** are higher than bleomycin (positive control) showing following tail moment values: 16 ± 0.6, 28 ± 0.4 and 13 ± 0.6 for complex **1** and bleomycin, respectively.

In addition, complex **2** exert genotoxic effects showing a lesser effect than complex **1**. Besides, both complexes did not exert genotoxic effects on normal L929 fibroblast from 2.5 to 10 μM whilst cisplatin induced the break of cellular DNA in the same range of concentrations (see Figure 3B and Figure SM8). These results may explain the low cytotoxicity of both compounds on L929 cells in comparison with deleterious effects of cisplatin (see Table 2). In this sense, cisplatin has a well-known mechanism of interaction with DNA.

Altogether, these results suggest that the genotoxic effects of complex **1** are higher than complex **2** in Jurkat cells, leading to a positive result in the comet assay and in agreement with the result observed in Figure 2.

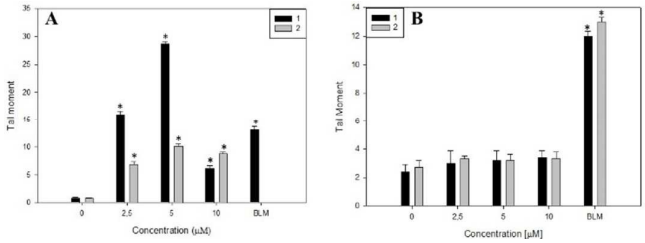

Figure 3. Genotoxicity of complexes **1** and **2** on Jurkat cells (A) and L929 cells (B) determined by SCGE (comet assay). DNA damage was evaluated by the tail moment. After incubation with both compound for 48 h, cells were lysed and DNA fragments were processed by electrophoresis. After that, the nuclei were stained and analyzed. Results are expressed as mean ± SEM (n = 150), *p < 0.001. BLM stands for bleomycin (10 μg/mL) used as a positive control.

Proteins

The binding of complex **1** with Lysozyme and RNase was evaluated with UV spectroscopy as described in the experimental part. The k' was calculated as a pseudo first order reaction (k'_{RNase}: and k'_{Lys}: $1.91x10^{-4}s^{-1}$ and $1.33x10^{-4}s^{-1}$) using the 3:1 stoichiometry (metal to protein) as the result were equal using the stoichiometry 10:1(metal to protein) (Figure SM6 and SM7). The rate constant of complex **1** with Lysozyme and RNase give us an estimation of the compatibility and reactivity of complex **1** in the presence of representative proteins of cellular media. We have used cisplatin as a control, and its values with lysozyme ($1.98{\cdot}10^{-4}$ s^{-1}) and RNase ($1.88{\cdot}10^{-4}$ s^{-1}) are in agreement with those found with other models such as albumin, transferrin, and cytochrome c.[37, 38] Complex **1**'s values are within the range found for cisplatin.

Interaction of the complexes with a proteasome target

In order to shed light on the mechanism of action for these complexes, and based on the lower reactivity with CT DNA, we evaluate a more specific target: proteasome. The ubiquitin-mediated proteasomal proteolysis is the main mechanism of degradation of proteins in human cells.[39] The 20S proteasome, which is the proteolytic core of the multicatalytic 26S

View Article Online
DOI: 10.1039/C7QI00446J

proteasome complex, has several proteolytic activities, including chymotrypsin-like, trypsin-like… etc.[40]
Nevertheless, it has been shown that only inhibition of the chymotrypsin-like activity is tightly associated with induction of tumor cell death programs.[41] Proteasome inhibitors cause a buildup of unwanted proteins in the cell, inducing cell death rapidly and selectively, TSCNs derivatives has been also reported to be inhibitors of this target.[42]
We performed a cell-free proteasome activity assay in the presence of each of these compounds at different concentrations (2.5 to 100 µM). As it can be seen in the Table 4, the gradual decrease in the fluorescence indicates the proteasome inhibition ability. Complexes **1** and **2** inhibits he chymotrypsin-like activity of purified 20S proteasome with different potencies since complex **2** was found to be the most potent inhibitor (see Table 4).

Table 4. Proteasome (chymotrypsin-like activity) inhibition percentage of complexes **1** and **2**

Concentration (µM)	**1** (% Basal ± SD)	**2** (% Basal ± SD)
2.5	97 ± 2	95 ± 1
5	94 ± 4	93 ± 1
10	73 ± 3	79 ± 3
25	73 ± 4	55 ± 4
50	69 ± 1	44 ± 2
100	51 ± 2	24 ± 2

In this order, Tundo and col. showed that cisplatin induces a dose dependent inhibition of the three activities of proteasome, at least over the concentration range investigated (2.5-15 µM). The described behaviors clearly demonstrate that cisplatin significantly affects the enzymatic properties of proteasome in vitro.[43]
On the other hand, we confirm the inhibitory effects of complex **1** and **2** on proteasome activity, we performed a cell proteasome activity experiments using Jurkat cells in the presence of 100 µM of complexes **1** and **2**. Proteasomal activity was inhibited to similar levels by both compounds. As it can be seen that the complex **1** reduced the proteasome activity in 28% whilst the complex **2** decreased the proteasome activity in 23% showing a similar proteasome inhibition effects.

ROS Production

Oxidative stress is one of the main factors reported that trigger the deleterious actions of metal-based compounds.[44, 45]
For a better understanding of the possible mechanism involved in the cytotoxicity of both complexes in cancer cell lines, we evaluated the effect of complexes **1** and **2** on oxidative stress through the oxidation of the probe DHR-123. DHR-123 is a mitochondria-associated probe that selectively reacts with hydrogen peroxide.[46] Incubation of Jurkat cells with the complex **1** caused an increase in the production of ROS. At 10 µM, complex **1** increased ROS production after 48 h generated 182% of ROS level over basal ($p<0.01$) whereas at 2,5 and 5 µM no production of ROS over the basal level could be observed ($p<0.01$). Moreover, the complex **2** does not exhibit a ROS production in the range of concentrations tested (2.5-25 µM) (see Figure SM9).

Apoptosis

Apoptosis is a physiological process of cell death enhanced in the presence of injurious agents. As a consequence, a genetic program that leads to cell death is activated. Apoptosis is characterized by some morphological changes in the nucleus and the cytoplasm. Because of this, apoptosis can be assessed by using several characteristic features of programmed cell death. Independently of the cell type and the nature of the harmful agent, the externalization of phosphatidylserine is always present in the earlier apoptotic events. Annexin V–FITC is a fluorescent probe with high affinity for phosphatidylserine, allowing its determination by fluorescence assays. Figure 4 depicted the flow cytometry results of the apoptotic process in the presence of complex **1** and **2** (10, 25, 50 and 100 µM) after 48 h of incubation in Jurkat cells.

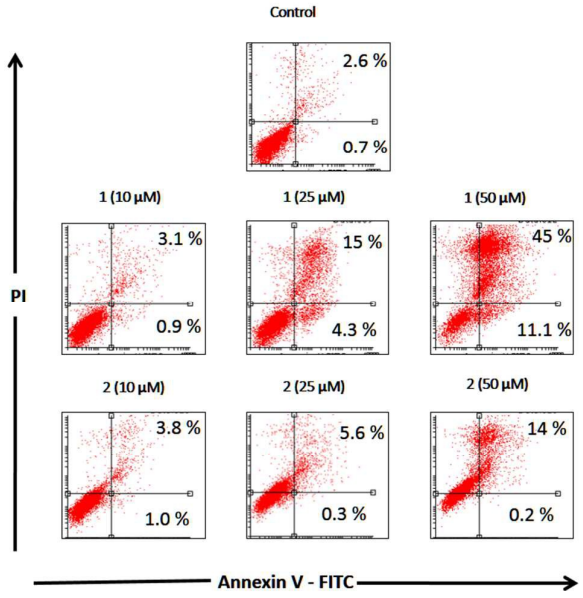

Figure 4. Induction of apoptosis in Jurkat cells. The panels show the cell distribution revealed by the intensity of PI-derived fluorescence and annexin V positive, in untreated cell cultures (Control) and cultures treated for 48 h in the presence of complex **1** and **2** (10, 25, 50 and 100 µM).

Table 5 displays the quantification of early and late stages of apoptosis obtained by flow cytometry in Jurkat cells. This table shows that the control cultures showed 0.7% of early apoptotic cells and 2.6 % of late apoptotic cells. These results changed when incubated the cells with 10, 25 and 50 µM of complex **1** and **2**, showing an increase in the early and late apoptotic cellular fraction.
Complex **1** resulted in approximately 4.3% and 11.1 % early apoptotic cells (annexin V positive) at 25 µM and 50 µM, respectively, whilst complex **2** did not show any changes in early apoptotic fractions over basal at 10, 25 and 50 µM.
Nevertheless, both compounds increased late apoptotic fractions, complex **1** produced 15.4% and 45.2 % at 25 µM and 50 µM whilst complex **2** resulted in 5.6 % and 13.9 % at the same concentrations.

View Article Online
DOI: 10.1039/C7QI00446J

As can be seen, the percentages of apoptotic and apoptotic/necrotic cells increased with the concentration of both complexes. These results are in accordance with the viability assays, confirming that the deleterious action of complex **1** are higher than complex **2**

Table5. Percentage of apoptotic cells treated with complexes **1** and **2**.

	Annexin V+/PI-		Annexin V+/PI+	
Concentration(μM)	**1 (%)**	**2 (%)**	**1 (%)**	**2 (%)**
0	0.7	0.7	2.6	2.6
10	0.9	1	3.1	3.8
25	4.3	0.3	15.4	5.6
50	11.1	0.2	45.2	13.9

On the other hand, caspases (cysteine-requiring aspartate proteases) are a family of proteases that mediate cell death and are important to the process of apoptosis. Caspase 3 is one of the critical members of this family. It is an effector caspase that cleaves most of the caspase-related substrates involved in apoptosis regulation.[47]

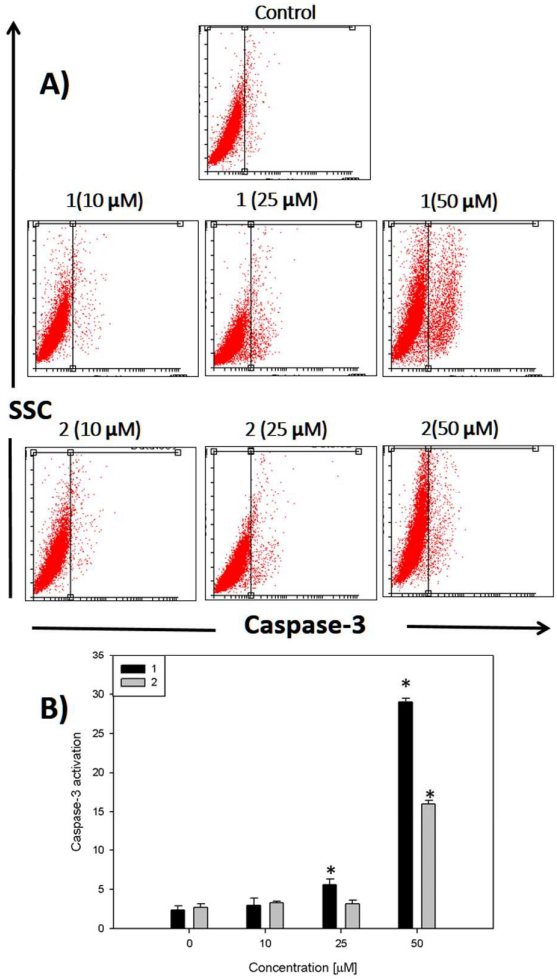

Figure 5. Induction of apoptosis in Jurkat cells. A) the panels show the cell distribution with SSC and caspase-3 levels, in untreated cell cultures (Control) and cultures treated for 48 h in the presence of compound **1** and **2** (10, 25 and 50 μM). B) caspase 3 activation versus complex **1** and **2** concentration graph

In Figure 5, it can be seen that after 48 h of incubation of the cells with complex **1** and complex **2**, caspase 3 is activated at 25 and 50 μM for compound **1** and only at 50 μM for compound **2** ($p<0.01$), demonstrating that the apoptotic action of both complexes is in agreement with the annexin V assay. The activation of caspase 3 is a good marker to confirm the annexin V results for the detection of late apoptosis.

Experimental

Materials and methods

In general, solvents and starting materials were purchased from the commercial companies: VWR and Aldrich –Sigma. In particular, the proteasome was purchased from Merck and plasmid pBR322 from GenCust.

Tissue culture materials were purchased from Corning, Dulbecco´ s Modified Eagles Medium (DMEM), TrypLE™ from Gibco and fetal bovine serum (FBS) from Internegocios SA. Dihydrorhodamine 123 (DHR) was purchased from Molecular Probes (Eugene, OR). Syber Green and Low melting point agarose were purchased from Invitrogen Corporation.

Mono-dimensional ^{13}C-NMR and ^{1}H-NMR experiments were performed in DMSO-d^6 and D_2O using a Bruker AMX-300 (300 MHz) spectrometer at room temperature (25 °C). Elemental analyses were performed on a Perkin Elmer 2400 Series II microanalyzer. Fast atom bombardment (FAB) mass spectrum (MS) was performed on a VG AutoSpec spectrometer. IR was performed in a Perkin Elmer Model 283 spectrophotometer with an ATR accessory (Miracle Single Reflection Horizontal). UV-Visible in a Thermo Fisher Scientific Evolution 260 Bio spectrophotometer.

Chemistry

Pyrrol-2-carboxaldehyde ^{4}*N*-*p*-chlorophenilthiosemicarbazone LH_2

^{4}*N*-*p*-chlorophenylthiosemicarbazide preparation was performed following a procedure used for similar compounds[48]: 20 mL of an ethanolic solution of hydrazine monohydrate (0.25 g, 5 mmol) was added dropwise and with constant stirring to a 20mL of a cold ethanol solution of *p*-chlorophenyl isothiocyanate (0.85 g, 5 mmol). The solution was allowed to stand until a white solid precipitation formed. The final compound was filtered off, washed with cold ethanol and diethyl ether and dried *in vacuo*. Yield 41% (0.41 g). The compound was achieved previously and characterized by X-ray, but there are no reports in the reference of further characterization of this compound using the usual spectroscopic and analytical techniques. The characterization is included as follows:

Mp 180 ºC. Elemental analysis found, C, 41.70; H, 4.15; N, 20.80; S, 16.11; $C_{12}H_{11}N_4SCl$ requires C, 41.70; H, 4.00, N, 20.85; S, 15.85 %. IR (KBr pellet): υ/cm-1 3293, 3178 (s, NH); 1635 (s, NH_2); 820 (w, CS-thioamide IV). ^{1}H NMR (d6-DMSO, ppm), δ=9.19 [s, NH, 1H]; 7.70, 7,67 (d, J = 9.0 Hz, CH, 2H); 7.34; 7.31 (d, J = 9.0 Hz, CH, 2H).

Thought the procedure was first reported in the fifties[19] later on slightly changed for α-N- heterocycles thiosemicarbazones

View Article Online
DOI: 10.1039/C7QI00446J

and it proceeds as follows[49]: *p*-chlorophenylthiosemicarbazide LH_2 (0.403 g, 2 mmol) was dissolved in 20 mL of ethanol and 5 mL of warm water at 40ºC. The clear solution was added dropwise to an ethanolic solution (10 mL) of pyrrol-2carboxaldehyde (0.19 g, 2 mmol). The reaction was heated to reflux for 5h (~78 ºC), afterwards the reaction was taken to the rotavapor and concentrated to half of the volume until a yellow solid precipitates which was isolated by filtration, washed with ethanol and dried.

Yield: 51% (0.284 g). Mp 195 °C (decomposes). Elemental analysis found, C, 51.20; H, 4.00; N, 19.70; S, 11.80; $C_{12}H_{11}N_4SCl$ requires C, 51.70; H, 3.95, N, 20.10; S, 11.50 %. MS (FAB+ with mNBA: nitrobenzyl alcohol matrix) m/z 279 for $[H_2L+H]^+$. IR (KBr pellet): υ/cm^{-1} 3291, 3225, 3151 (m, NH); 1609 (s, CN); 820 (w, CS-thioamide IV). ^{1}H NMR (d^6-DMSO, ppm), δ=11.78 [s, 3NH, 1H]; 11.52 [s, 2NH, 1H]; 10.06 [s, 4NH, 1H]; 7.99 [s, 1CH, 1H]; 7.68, 7,65 (d, *J* = 9.3 Hz, 9CH, 11CH, 2H); 7.47; 7.44 (d, *J* = 9.3 Hz, 8CH, 12CH, 2H); 7.09 [s, 5CH, 1H]; 6.48 [s, 4CH, 1H]; 6.15 [s, 3CH, 1H]. ^{13}C NMR (d^6-DMSO, ppm), δ=176.08 (C6); 139.29 (C7); 135.91 (C2); 130.38 (C1); 129.44 (C9, C11); 128.66 (C10); 127.97 (C8, C12); 123.57 (C5); 115.19 (C3); 110.85 (C4). UV/vis (DMSO UV/vis (DMSO): λ/nm 287 (IL π−π*), 347 (IL n −π*).

Complexes 1 and 2

Complex **1**, $[Pd(LH)_2]$. A solution of LH_2 (0.143 g; 0.50 mmol) in methanol (MeOH) (20 mL) was added dropwise to a solution of Li_2PdCl_4, prepared in situ, from $PdCl_2$ (0.044 g; 0.25 mmol) and LiCl (0.004 g; 1 mmol) in methanol (20 mL). The mixture was kept stirring at room temperature for 2 hours. The final solid was isolated by filtration. Then washed with hot MeOH, dried under vacuum into a dry oven at 60°C. 0,142 g (yield: 86%).

Yield: 86% (0.142 g). Mp >250 °C. Elemental analysis found, C, 40.15; H, 3.30; N, 15.35; S, 8.90; $C_{24}H_{20}N_8S_2Cl_2Pd•3H_2O$ requires C, 40.25; H, 3.65, N, 15.65; S, 8.95 %. MS (FAB+ with mNBA: nitrobenzyl alcohol matrix) m/z 663 for $[H_2L+H]^+/[M]^+$. IR (KBr pellet): υ/cm^{-1} 3228 (m, NH); 1598 (s, CN); 827 (w, CS-thioamide IV). ^{1}H NMR (d^6-DMSO, ppm), δ=11.54 [s, 3NH, 1H]; 9.48 [s, 4NH, 1H]; 7.49 [s, 1CH, 1H]; 7.42-7,32 [m, 8CH, 9CH, 11CH, 12CH, 4H]; 7.17 [s, 5CH, 1H]; 6.91 [s, 4CH, 1H]; 6.26 [s, 3CH, 1H]; ^{13}C NMR (d^6-DMSO, ppm), δ=169.44 (C6); 146.87 (C7); 140.28 (C2); 129.19 (C9, C11); 129.06 (C1); 127.37 (C10); 123.14 (C8, C12); 12213 (C5); 120.21(C3); 111.18 (C4). λ/nm 270 (IL π−π*), 389 (CT Metal-L). Single crystals, suitable for X-ray diffraction analysis, grown in a NMR tube from the d^6-DMSO solution used for NMR experiments.

Complex **2**, $[Pt(LH)_2]$. 5mL of an aqueous solution of K_2PtCl_4 (0.104 g, 0.25 mmol) was added dropwise to a methanolic solution (20 mL) of LH_2 (0.140 g, 0.5 mmol). The mixture was stirred at room temperature during 5h. The final solid was filtered, washed with hot methanol and dried under vacuum.

Yield: 58% (0.187 g). Mp >250 °C. Elemental analysis found, C, 36.30; H, 3.05; N, 13.80; S, 8.00; $C_{24}H_{20}N_8S_2Cl_2Pt•2H_2O$ requires C, 36.65; H, 3.05, N, 14.25; S, 8.15 %. MS (FAB$^+$ with mNBA: nitrobenzyl alcohol matrix) m/z 751 for $[H_2L+H]^+$. IR (KBr pellet): υ/cm^{-1} 3226 (m, NH); 1608 (s, CN); 827 (w, CS-thioamide IV). ^{1}H NMR (d^6-DMSO, ppm), δ=11.57 [s, 3NH, 1H]; 9.61 [s, 4NH, 1H]; 7.46 [s, 1CH, 1H]; 7.35-7,25 [m, 8CH, 9CH, 11CH, 12CH, 4H]; 7.07 [s, 5CH, 1H]; 6.50 [s, 4CH, 1H]; 6.16 [s, 3CH, 1H]; ^{13}C NMR (d^6-DMSO, ppm), δ=175.15 (C6); 138.41 (C7); 135.01 (C2); 129.44 (C1); 128.52 (C9, C11); 127.76 (C10); 127.10 (C8, C12); 122.69 (C5); 114.29 (C3); 109.93 (C4). (DMSO): λ/nm 266(IL π−π*), 355(CT Metal-L).

Stability studies by UV and NMR

Complexes **1** and **2** have been monitored from fresh to 24h in solution where the pH was adjusted to the physiological range, using the appropriate buffer solutions (Tris-HCl 0.5M Tris Base pH:7.6).

Crystallography

Data were collected on a Bruker Kappa Apex II diffractometer. A summary of the crystal data, experimental details and refinement results is listed in Table 6. The software package SHELXTL was used for space group determination, structure solution, and refinement.[50] The structure was solved by direct methods, completed with difference Fourier syntheses, and refined with anisotropic displacement parameters.

Table 6. Crystal and refinement data for $[Pd(LH)_2)]·2DMSO$.

	$[Pd(LH)_2]·2DMSO$	
Chemical formula	$C_{228}H_{32}Cl2N_8O_2PdS_4$	
Formula weight	409.08 g/mol	
Temperature	296(2) K	
Wavelength	0.71073 Å	
Crystal size	0.050 x 0.060 x 0.190 mm	
Crystal habit	orange needle	
Crystal system	monoclinic	
Space group	P 1 21/c 1	
Unit cell dimensions	a = 14.627(4) Å b= 5.7150(18) Å c = 20.939(7) Å	α = 90º β = 4.995(10)º γ = 90º
Volume	1743.7(9) Å^3	
Z	2	
Density (calculated)	1.558 g/cm^3	
Absorption coefficient	0.964 mm^{-1}	
Theta range for data collection	1.95 to 25.37°	
Index ranges	-17<=h<=17; -6<=k<=6; -25<=l<=25	
Reflections collected	26868	
Independent reflections	3189 [R(int) = 0.0538]	
Coverage of independent reflections	99.9%	
Data / restraints / parameters	3189 / 0 / 207	
Goodness-of-fit on F^2	1.083	
Final R indices	*I* > 2σ(I): R1 = 0.0403, wR2= 0.1064 all data : R1 = 0.0682, wR2 = 0.1297	
Largest diff. peak and hole	0.700 and -0.665 e Å^3	

Biology

Cell line and growth conditions

View Article Online
DOI: 10.1039/C7QI00446J

MG-63 human osteosarcoma cells, A549 human lung adenocarcinoma cells and L929 mouse fibroblasts were grown in DMEM containing 10 % FBS, 100 U/mL penicillin and 100 µg/mL streptomycin at 37ºC in 5% CO_2 atmosphere. Cells were seeded in a 75 cm^2 flask and when 70-80 % of confluence was reached, cells were subcultured using 1mL of TrypLE TM per 25 cm^2 flask. For experiments, cells were grown in multi-well plates. When cells reached the desired confluence, the monolayers were washed with DMEM and were incubated under different conditions according to the experiments. On the other hand, Jurkat cells (acute T cell leukemia) were grown in DMEM containing 10 % FBS, 100 U/mL penicillin and 100 µg/mL streptomycin at 37ºC in 5% CO_2 atmosphere. For experiments, cells were grown in multi-well plates according to the experiments.

Cytotoxicity by MTT assay

The MTT assay was performed according to Mosmann et al.[51] Briefly, cells were seeded in a 96-multiwell dish, allowed to attach for 24 h and treated with different concentrations of complex 1 and 2 at 37 °C for 48 and 72 h. After that, the medium was changed and the cells were incubated with 0.5 mg/mL MTT under normal culture conditions for 3 h. Cell viability was marked by the conversion of the tetrazolium salt MTT (3-(4, 5-dimethylthiazol-2-yl)-2,5-diphenyl-tetrazolium-bromide) to a coloured formazan by mitochondrial dehydrogenases. Colour development was measured spectrophotometrically in a Microplate Reader (7530, Cambridge technology, Inc, USA) at 570 nm after cell lysis in DMSO (100 µL/well). Cell viability was plotted as the percentage of the control value.

DNA and protein interaction

Sample preparation

In order to evaluate the biological behaviour of complexes **1-2**, the compounds were initially dissolved in DMSO (5 mM). For all experiments, the desired concentration of complexes was achieved by dilution of the stock DMSO solution with aqueous buffer. All the solutions and buffers were previously tempered to 37 ºC. Afterward, the fresh prepared complexes solutions were mixed at 37 ºC with the aqueous buffer DNA/model protein solutions in a thermoshaker. The studies never exceeded 1% DMSO (v/v) in the final solution. Control experiments with DMSO were performed and no changes in the spectra of the model proteins or CT DNA were observed.

UV/Vis titration experiments

To investigate the potential binding ability of complexes 1-2 with DNA spectrophotometric titrations (240-800nm) were performed at room temperature by: a) keeping constant the CT-DNA concentration (3.2×10^{-5} M) while varying the concentration of each complex (0-500 µM) and monitoring the changes in the typical absorbance of CT-DNA at 260 nm after equilibration (10 min. At 37ºC), b) keeping constant the complex concentration (2.5×10^{-6} M), varying the concentration of CT-DNA (0–500 µM) and monitoring the changes in the absorbance of one characteristic charge transfer band of the complex after equilibration (10 min. At 37ºC). The first assay was used to estimate the nature of the supramolecular interactions while the latter assay was used to determine the DNA-binding constant of the complexes, Kb (in M^{-1}) using the Wolfe-Shimer equation:[32]

$$\frac{[\mathrm{DNA}]}{\varepsilon_a - \varepsilon_f} = \frac{[\mathrm{DNA}]}{\varepsilon_b - \varepsilon_f} + \frac{1}{K_b(\varepsilon_b - \varepsilon_f)}$$

where [DNA] is the concentration of the nucleic acid in base pairs, ε_a is the apparent absorption coefficient obtained by calculating A_{obs}/[compound], and ε_f and ε_b are the absorption coefficients of the free and the fully bound compound, respectively.

Agarose gel electrophoresis

Complex **1** was incubated at 37ºC with a concentration of 0.0625µg/µL of pBR322 plasmid DNA, at different concentrations expressed as r_i= Complex: DNA(base pair) ratio. The r_i used is from 0.01 to 0.2, in a total volume of 20µL.
After an incubation period of 24 and 48 h, the mobility of the complex treated pBR322 samples was analyzed by gel electrophoresis at 70 V/cm in Tris-acetate/EDTA buffer. A control of pBR322 was also incubated, and load of a 1kb ladder5mL was also loaded in lane 1 of the gel. The gel was stained with an ethidium bromide aqueous solution and DNA bands were visualized with a UV-transilluminator. pBR322 was purchased from GenCust and the 1kb ladder from Aldrich-sigma (D0428).

Single cell gel electrophoresis (SCGE) assay

For the detection of DNA strand breaks the single cell gel electrophoresis ('comet') assay was used in the alkaline version, based on the method of Singh et al.[52] with minor modifications. Under alkaline conditions, DNA loops containing breaks lose supercoiling, unwind and are released from the nuclei and form a 'comet-tail' by gel electrophoresis. For this experiment, 2×10^4 cells were seeded in a twelve-well plate; 24 h later the cells were incubated with various concentrations of the complexes. After treatment, cells were suspended in 0.5% low melting point agarose and immediately poured onto glass microscope slides. Slides were immersed in an ice-cold prepared lysis solution at darkness for 1 h (4 °C) in order to lyse the cells, remove cellular proteins and to permit DNA unfolding. Immediately after this, slides were put in a horizontal electrophoresis tank containing 1 mM Na_2EDTA, 0.3 M NaOH (pH 12.7) and then electrophoresis was performed for 30 min at 25 V (4 °C). Afterwards, slides were neutralized and stained with Syber Green. Analysis of the slides was performed in an Olympus BX50 fluorescence microscope. Cellular images were acquired with a Leica IM50 Image Manager (Imagic Bildverarbeitung AG). A total of 50 randomly captured cells per experimental point of each experiment was used to determine the tail moment (the product of tail length by tail DNA percentage) using a free comet scoring software (Comet Score version 1.5). Two parallel slides were performed for each experimental point. Independent experiments were

View Article Online
DOI: 10.1039/C7QI00446J

repeated twice. A pulse of 20 minutes of 10 μg mL^{-1} bleomycin just before the cells were harvested was employed as the positive control.

UV/Vis kinetics experiments

To investigate the interaction of complex **1** with plasma proteins, electronic spectra of the protein models, HEWL (hen egg white lysozyme) and RNase A at 10^{-5} M were recorded (monitoring the typical absorbance of proteins at 280 nm) before and after the addition of complex 1 at a stoichiometric ratio of 3:1 (metal to protein) for 24 h at R.T. The binding affinity constants were calculated as a pseudo first order based on the equal results obtained for stoichiometry: 10:1 and 3:1 for both cases.[53]

Proteasome activity assay

Proteasomal inhibition by complexes **1-2** was assayed using the 20S Proteasome Activity Assay Kit from Millipore. To determine whether both compounds inhibits proteasome function directly, the provided 20S proteasome was diluted 1:60 in 100μl assay buffer and incubated according to the manufacturer's instructions with the suc-LLVY-AMC substrate and the indicated concentrations of complexes **1-2** for 2 h at 37°C. Fluoresence at 460 nm was read using a FluoSTAR OPTIMA microplate reader.

Moreover, Jurkat whole-cell extract (8 μg) was incubated with 10 μmol/L chymotrypsin-like-substrate (Suc-LLVY-AMC) in 100 μL assay buffer [50 mmol/L Tris-HCl (pH 7.5)] in the presence of both compounds (100 μM each) or solvent DMSO as control. After a 2 h incubation at 37° C, production of hydrolyzed AMC groups was measured using a spectrofluorophotometer shimadzu RF-6000 with an excitation filter of 365 nm and an emission filter of 460 nm.

Determination of Reactive Oxygen Species (ROS) Production

Oxidative stress in Jurkat cells was evaluated by measurement of intracellular production of reactive oxygen species (ROS) after incubation of the cells with different concentrations (2.5-25 μM) of the complex **1** in water (from 20 mM of stock solution in DMSO) during 48 h at 37 °C. ROS generation was determined by oxidation of DHR-123 to rhodamine by spectrofluorescence as we have previously described[54].

Measurements of externatization of phosphatidylserine by annexin V-FITC/PI staining

Cells in early and late stages of apoptosis were detected with annexin V–FITC and PI staining. Cells were treated with different concentrations of compound **1** and **2** and were incubated for 48 h prior to analysis. Cells were analyzed using a BD FACS Calibur™ flow cytometer and FlowJo 7.6 software. For each analysis, 10,000 counts, gated on a forward scatter versus side scatter dot plot, were recorded. Four subpopulations were defined in the dot plot: the undamaged vital (annexin V negative/PI negative), the vital mechanically damaged (annexin V negative/PI positive), the apoptotic (annexin V positive/PI negative), and the secondary necrotic (annexin V positive/PI positive) subpopulations.

Caspase 3 assay:

The determination of caspase 3, one of the main effector caspases, was conducted with a commercial kit (Pharmingen TM caspase 3 assay kit, BD) following the recommendation of the manufacturer. The cells (10,000 events) were analyzed using a BD FACS Calibur™ flow cytometer and FlowJo 7.6 software.

Conclusions

The synthesis of complexes using Palladium and Platinum as metals with a heterocyclic thiosemicarbazone derivative has afforded two new mononuclear structures, which in both cases, showed a good stability in solution and biological buffers. The compounds interact not only with DNA models (pBR322 and CT DNA) but also with protein (lysozyme and RNase models) showing different values of interaction and following a different pattern than cisplatin. Both compounds caused cytotoxicity in a concentration- dependent manner on several tumor cell lines included leukemia and different solid tumors (lung and bone). The important pharmacological fact is that both compounds showed high selectivity for tumor cells and no activity versus healthy cells such as normal L929 fibroblast.

Moreover, the palladium complex **1** is not only endowed with a higher cytotoxicity than the platinum complex **2** but also with potent inhibition capacity of proteasome 20S. With these data on hand, we can establish that the mechanism of these complexes must be quite different to cisplatin.

As a whole, these results indicate that compound, **1** is an interesting candidate for potential antitumor uses, and provide new insight into the development of palladium compounds as potential anticancer agents.

Acknowledgements

This work was supported by the following grants for the Spanish MINECO: SAF-2012-34424, CTQ2015-68779R and CTQ2015-70371-REDT. We thank Prof. J. Satrustegui from CBMSO for the use of the fluorescence equipment and the Secretary of University Policies (SPU, Argentina) for IEL's travel fellowship.

References

1. C. R. Kowol, R. Trondl, P. Heffeter, V. B. Arion, M. A. Jakupec, A. Roller, M. Galanski, W. Berger and B. K. Keppler, *J Med Chem*, 2009, **52**, 5032-5043.
2. C. A. Kunos, T. Radivoyevitch, S. Waggoner, R. Debernardo, K. Zanotti, K. Resnick, N. Fusco, R. Adams, R. Redline, P. Faulhaber and A. Dowlati, *Gynecol Oncol,* 2013, **130**, 75-80.
3. USA (Bethesta).Pat, NCT01835171 (NCI), **2016**.
4. E. Colleen Moore and A. C. Sartorelli, *Pharmacol Ther*, 1984, **24**, 439-447.
5. W. E. Antholine, J. M. Knight and D. H. Petering, *J Med Chem*, 1976, **19**, 339-341.

DOI: 10.1039/C7QI00446J

6. M.-C. Liu, T.-S. Lin, A. C. Sartorelli, G. P. Ellis and D. K. Luscombe, in *Prog Med Chem*, Elsevier, 1995, vol. Volume 32, pp. 1-35.
7. C. R. Kowol, R. Berger, R. Eichinger, A. Roller, M. A. Jakupec, P. P. Schmidt, V. B. Arion and B. K. Keppler, *J Med Chem*, 2007, **50**, 1254-1265.
8. C. R. Kowol, W. Miklos, S. Pfaff, S. Hager, S. Kallus, K. Pelivan, M. Kubanik, Ã. v. A. Enyedy, W. Berger, P. Heffeter and B. K. Keppler, *J Med Chem*, 2016, **59**, 6739-6752.
9. A. G. Quiroga and C. N. Ranninger, *Coord Chem Rev*, 2004, **248**, 119-133.
10. A. G. Quiroga, J. M. Perez, I. Lopez-Solera, J. R. Masaguer, A. Luque, P. Roman, A. Edwards, C. Alonso and C. Navarro-Ranninger, *J Med Chem*, 1998, **41**, 1399-1408.
11. A. G. Quiroga, J. M. Perez, E. I. Montero, J. R. Masaguer, C. Alonso and C. Navarro-Ranninger, *J Inorg Biochem*, 1998, **70**, 117-123.
12. A. I. Matesanz, P. Albacete, J. Perles and P. Souza, *Inorg Chem Front*, 2015, **2**, 75-84.
13. K. A. Price, A. Caragounis, B. M. Paterson, G. Filiz, I. Volitakis, C. L. Masters, K. J. Barnham, P. S. Donnelly, P. J. Crouch and A. R. White, *J Med Chem*, 2009, **52**, 6606-6620.
14. Y. Yu, D. S. Kalinowski, Z. Kovacevic, A. R. Siafakas, P. J. Jansson, C. Stefani, D. B. Lovejoy, P. C. Sharpe, P. V. Bernhardt and D. R. Richardson, *J Med Chem*, 2009, **52**, 5271-5294.
15. A. I. Matesanz, C. Hernández, J. Perles and P. Souza, *J Organomet Chem*, 2015, **804**, 13-17.
16. Y. Yu, J. Wong, D. B. Lovejoy, D. S. Kalinowski and D. R. Richardson, *Clin Cancer Res*, 2006, **12**, 6876-6883.
17. J. L. Hickey, J. L. James, C. A. Henderson, K. A. Price, A. I. Mot, G. Buncic, P. J. Crouch, J. M. White, A. R. White, T. A. Smith and P. S. Donnelly, *Inorg Chem*, 2015, **54**, 9556-9567.
18. A. Billiau, V. G. Edy, H. Heremans, J. Van Damme, J. Desmyter, J. A. Georgiades and P. De Somer, *Antimicrob Agents Chemother*, 1977, **12**, 11-15.
19. P. P. T. Sah and T. C. Daniels, *Rec.Trav.Chim.Pays Bas*, 1950, **69**, 1545-1556.
20. V. Martichonok, in *Encyclopedia of Reagents for Organic Synthesis*, John Wiley & Sons, Ltd, 2001.
21. A. I. Matesanz, J. Perles and P. Souza, *Dalton Trans*, 2012, **41**, 12538-12547.
22. W. Hernandez, A. J. Vaisberg, M. Tobar, M. Alvarez, J. Manzur, Y. Echevarria and E. Spodine, *New J Chem*, 2016, **40**, 1853-1860.
23. A. I. Matesanz, I. Leitao and P. Souza, *J Inorg Biochem*, 2013, **125**, 26-31.
24. A. R. Kapdi and I. J. S. Fairlamb, *Chem Soc Rev*, 2014, **43**, 4751-4777.
25. D. A. Tocher, *Appl Organomet Chem*, 2000, **14**, 172-173.
26. T. C. Johnstone, K. Suntharalingam and S. J. Lippard, *Chem Rev*, 2016.
27. A. Casini and J. Reedijk, *Chem Sci*, 2012, **3**, 3135-3144.
28. S. Medici, M. Peana, V. M. Nurchi, J. I. Lachowicz, G. Crisponi and M. A. Zoroddu, *Coordin Chem Rev*, 2015, **284**, 329-350.
29. G. Psomas, *J Inorg Biochem*, 2008, **102**, 1798-1811.
30. A. Meenongwa, R. F. Brissos, C. Soikum, P. Chaveerach, P. Gamez, Y. Trongpanich and U. Chaveerach, *New J Chem*, 2016, **40**, 5861-5876.
31. K. Nakamoto, M. Tsuboi and G. D. Strahan, in *Drug–DNA Interactions*, John Wiley & Sons, Inc., 2008, pp. 303-356.
32. A. Wolfe, G. H. Shimer and T. Meehan, *Biochemistry*, 1987, **26**, 6392-6396.
33. I. Haq, *Arch Biochem and Biophys*, 2002, **403**, 1-15.
34. G. L. Cohen, W. R. Bauer, J. K. Barton and S. J. Lippard, *Science*, 1979, **203**, 1014-1016.
35. A. R. Collins, V. L. Dobson, M. r. Dusinska, G. Kennedy and R. Stetina, *Mut Res*, 1997, **375**, 183-193.
36. W. Liao, M. A. McNutt and W.-G. Zhu, *Methods*, 2009, **48**, 46-53.
37. A. R. Timerbaev, C. G. Hartinger, S. S. Aleksenko and B. K. Keppler, *Chem Rev*, 2006, **106**, 2224-2248.
38. L. Messori, A. Casini, C. Gabbiani, E. Michelucci, L. Cubo, C. Rios-Luci, J. M. Padron, C. Navarro-Ranninger and A. G. Quiroga, *ACS Med Chem Lett*, 2010, **1**, 381-385.
39. R. Z. Orlowski and E. C. Dees, *Breast Cancer Res*, 2003, **5**, 1-7.
40. J. Sun, S. Nam, C.-S. Lee, B. Li, D. Coppola, A. D. Hamilton, Q. P. Dou and S. d. M. Sebti, *Cancer Research*, 2001, **61**, 1280-1284.
41. J. Adams, V. J. Palombella, E. A. Sausville, J. Johnson, A. Destree, D. D. Lazarus, J. Maas, C. S. Pien, S. Prakash and P. J. Elliott, *Cancer Res*, 1999, **59**, 2615-2622.
42. J. H. Gundelach, A. A. Madhavan, P. J. Wettstein and R. J. Bram, *The FASEB J*, 2012, **27**, 782-792.
43. G. R. Tundo, D. Sbardella, C. Ciaccio, S. De Pascali, V. Campanella, P. Cozza, U. Tarantino, M. Coletta, F. P. Fanizzi and S. Marini, *J Inorg Biochem*, 2015, **153**, 253-258.
44. I. E. Leon, A. L. Di Virgilio, D. A. Barrio, G. Arrambide, D. Gambino and S. B. Etcheverry, *Metallomics*, 2012, **4**, 1287-1296.
45. J. Rivadeneira, A. L. D. Virgilio, D. A. Barrio, C. I. Muglia, L. Bruzzone and S. B. Etcheverry, *Med Chem*, 2010, **6**, 9-23.
46. M. A. M. Capella, L. S. Capella, R. C. Valente, M. Gefa and A. G. Lopes, *Cell Biol and Toxicol*, 2007, **23**, 413-420.
47. H. Sakahira, M. Enari and S. Nagata, *Nature*, 1998, **391**, 96-99.
48. A. A. Hassan, E. M. El-Sheref and A. H. Abou-Zied, *J Het Chem*, 2011, **49**, 38-58.
49. F. E. Anderson, C. J. Duca and J. V. Scudi, *JACS*, 1951, **73**, 4967-4968.
50. SHELTXTL-NTversion 6.12, Structure Determination Package, Bruker-Nonius XS,Madison, Wishconsin USA, 1997−2001.
51. T. Mosmann, *J Immunol Methods*, 1983, **65**, 55-63.
52. N. P. Singh, M. T. McCoy, R. R. Tice and E. L. Schneider, *Exp Cell Res*, 1988, **175**, 184-191.
53. T. Marzo, G. Bartoli, C. Gabbiani, G. Pescitelli, M. Severi, S. Pillozzi, E. Michelucci, B. Fiorini, A. Arcangeli, A. r. G. Quiroga and L. Messori, *BioMetals*, 2016, **29**, 535-542.
54. I. E. Leon, A. L. Di Virgilio, V. Porro, C. I. Muglia, L. G. Naso, P. A. M. Williams, M. Bollati-Fogolin and S. B. Etcheverry, *Dalton Trans*, 2013, **42**, 11868-11880.